Analysis of Deformation Characteristics of AZ31B Friction Heating Incremental Forming

Wang jiahao

□□□□

Zhou Liuru (zlrhust@163.com)

Hu Shiyao

Nanchang University

Original Article

Keywords: Friction heating, Incremental forming, AZ31B, Finite element analysis, Deformation characteristics

Posted Date: July 20th, 2020

DOI: https://doi.org/10.21203/rs.3.rs-42757/v1

Abstract

A friction heating incremental forming (FHIF) is proposed, which does not require external heating. By means of orthogonal experimental, finite element analysis and CATIA reverse engineering methods, the forming characteristics of magnesium alloy AZ31B FHIF are studied, such as forming limit angle, dimensional accuracy, thickness distribution, equivalent stress and equivalent strain at different forming stages. The results show that: For the FHIF, the forming limit angle can be up to 76°, and the most obvious way to increase the forming limit angle is to increase the spindle speed. In the FHIF, due to the limitations of the experimental conditions, it will be different from the ideal model. The bending phenomenon first occurs in the early stage of forming, which makes the upper corner part the worst accuracy, and the lower corner part obvious defects. Compared with the theoretically stable thickness, the actual part sidewall is thinned by 11%. The simulation successfully predicts and observes the thickness change and stress-strain change trend of the entire FHIF.

1 Introduction

Magnesium alloys are difficult to process at room temperature and generally require heating [1, 2]. To overcome these challenges, a few forming processes have been conducted to address those issues. An effective solution is to employ a forming process at high temperatures [3, 4].The friction heating incremental forming (FHIF) is used to improve the plasticity of the magnesium alloy and save the cost of heating equipment. In the past ten years, scholars have continuously explored the research on the incremental forming process, but there are still many problems in the processing efficiency, surface quality, and geometric accuracy of parts. The incremental forming process has a long history and has great advantages over traditional processes [5, 6].

Most scholars are studying the incremental forming process of Al alloys. Shrivastava P et al. to observe the effect of strain levels, three different types of SPIF parts were formed that were subjected to early, intermediate and final forming stages. Further, microstructural and textural changes in the formed parts were identified for plane strain and biaxial strain deformation modes [7]. Kim T J et al. research findings that the uniformity of thickness throughout the deformed region is one of the key factors to improve the formability, and the double-pass forming method is found to be very effective [8]. Some scholars studied the influence of forming parameters on forming performance, the research work allowed identifying a critical threshold for the ratio between the thickness of the sheet and the radius of the tool that distinguishes between fracture with and without previous necking, for large tool radius, the stabilizing effect of dynamic bending under tension seems to improve forming ability, and the less the tool radius, the more severe the plate damage and the lower the formability, the size of the surface roughness can be changed by vertical step size and the forming angle [9-11]. Some scholars use the cruciform biaxial tension test and a specific simulation analysis model to predict the fracture strain, and observed that bending is the main deformation mechanism that affects the behavior of materials in SPIF[12-14].

Over the past decades, warm incremental sheet forming has received attention for Mg alloy sheet forming [15, 16]. The forming process of AZ31B magnesium alloy was used the method of hot air heating [17], electropulse-assisted [18], heating furnace [19], electromagnetic [20] and oil bath heating [21]. Different heat-assisted methods have their strengths and weaknesses. The common weakness of the above method is that it requires expensive heating equipment. And the HFIF does not have this shortcoming, which does not require external heating, and according to current experimental results, the unique characterization of ISF process is its increased forming limit compared with conventional sheet forming processes [22-24].

To the best of our knowledge, the proposed approach has an extremely simple apparatus structure and is quite economical, yet experimental investigations on the approach are particularly rare all over the world. Therefore, one of the main objectives of the present paper is to explore an innovative and simple experimental setup to form Mg alloy sheets or other hard-to-form metallic materials. But there is not much research on the HFIF, in this work, by means of orthogonal experimental to study the forming limit angle of AZ31B FHIF, and by means of CATIA reverse engineering to study the dimensional accuracy and thickness distribution of parts in different forming stages, then compared with the simulation results to confirm the correctness of the simulation. The FHIF improve and supplement the incremental forming process of magnesium alloy, it is of great significance to the incremental forming technology of magnesium alloy.

2 Experimental And Simulation Modeling

2.1 Experimental

The material used in the experiment is AZ31B magnesium alloy sheet. The initial thickness of sheet is 1.6 mm. Square blanks of 250×250 mm2 were cut from the sheets. The chemical composition is given in Table 1.

Table 1 Chemical composition of the AZ31B magnesium alloy sheet

Chemical composition (in % mass fraction)						
Material	Mg	Al	Zn	Mn	Si	Cu
AZ31B	Balance	2.38	0.20	0.22	0.05	0.005

The experiment adopts negative forming and does not require mold support. It is mainly composed of forming tool, sheet, clamping plate, blank holder, as shown in Fig. 1. And Fig. 2 is shown the CAD model of the cone box to be formed on the three-axis CNC milling machine (HNC-21/22M) by FHIF. The forming tool was controlled by G code generated by Computer Aided Manufacturing, and the tool path is shown in Fig. 3.

In order to study the parts in FHIF, the wall angle of 45° was selected, and the process parameters values are given in Table 2.

Table 2 FHIF parameters

Tool diameter (mm)	Vertical step size (mm)	Rotational speed (RPM)	Tool feed rate (mm min^{-1})	Lubricating oil	Temperature (°C)	Sheet thickness (mm)
12	1	2000	1000	Lithium grease oil	100	1.6

In order to observe the different of the sheet metal during the entire forming process, it is usually necessary to evaluate the deformation characteristics of each period from the beginning to the end of the process. Qualitatively the FHIF stages are classified as the early forming stage, intermediate forming stage and final forming stage. Based on to pre-experimental investigations, the forming depth was chosen as 15mm, 30mm and 60mm respectively for the parts classified as early, intermediate and final stages of forming. Formed samples pertaining to different HFIF stages were digitized with the help of CATIA. Further, the samples were aligned with respective CAD parts to quantify the deviation, deviation and causes from ideal CAD parts was discussed. The geometric models and formed parts were subjected the early, intermediate and final forming stages are shown in Fig. 4.

2.2 Simulation Modeling

The progressive forming process is a complex elastoplastic large deformation process such as geometric nonlinearity, material nonlinearity and boundary condition nonlinearity. AQABUS software is used to establish the finite element model of AZ31B magnesium alloy FHIF, and the thinning and stress of the sheet metal wall during the forming process is analyzed.

In order to simulate this process, the material model parameters were evaluated through uniaxial tensile test of the dog bone samples. The universal material testing machine of Fig. 5a was used to measure the mechanical parameters of the material under different rolling directions. Fig. 5b and Fig. 5c show the dog bone samples size and the sample cut along the rolling direction of the sheet 0°, 45°, 90°. The model parameters with the temperature of 100°C are shown in Table 3, and the true stress-strain curves are shown in Fig. 6.

Table 3 Material performance parameters

	1	2	3
Temperature （°C）	100	100	100
Rolling Direction（°）	90	45	0
Yield Strength（MPa）	135	132	138
Tensile Strength（MPa）	187	210	207
Elongation （%）	44.0	44.0	48.5
Elastic Modulus（GPa）	27.3	27.2	33.5
Poisson's Ratio	0.378	0.369	0.372
Plastic Strain Ratio	5.12	4.26	3.58

Finite element analysis of FHIF process has been performed using AQABUS software. Mid surfaces of both the geometries were extracted and meshed in HyperMesh environment. For the meshing of the sheet, the four node shell element was adopted, and the thickness of the shell element was considered same as the initial thickness of the sheet (1.6mm). In FHIF, because the sheet remains fixed during operation the nodes present on the outer periphery of sheet were constrained in both translational and rotational motion in "X", "Y", and "Z" directions. The tool was constrained with rotation in the "X" and "Y" directions, and the rotation was allowed in the Z direction. Input the magnesium alloy material parameters measured above into the sheet node, the tool is considered as the rigid body and the tool path is assigned to the master node of the tool. The contact modeling of forming tool and sheet is shown in Fig. 7.

3 Results And Analysis

3.1 Forming limit analysis

"Orthogonal experiment design" is a scientific method of analyzing multi-factor experiments, which can greatly reduce the number of experiments and will not reduce the feasibility of experiments. The orthogonal experiment design was used to study the influence of forming parameters on the forming ability of the sheet metal. The three factors are the rotational speed, vertical step size, tool diameter, the level of the orthogonal experiment factors as shown in Table 4, and the angle and temperature when the sheet material was broken were recorded. The table of orthogonal experiment results was got, then the experimental data was analyzed, the impact of each process parameter on the forming performance was observed, and the relatively good set of process parameters for later test analysis was got.

Table 4 Orthogonal experimental factor level table

Forming parameters	Factor	Level					
		1	2	3	4	5	6
Rotational speed（rpm）	A	500	1000	1500	2000	2500	3000
Vertical step size（mm）	B	1	1.5	2			
Tool diameter（mm）	C	8	12	16			

In the HFIF, the angle α between the forming sheet and the vertical direction was the forming angle, as shown in Fig. 8. The thickness of the deformation zone conforms to the law of cosine $t=t^0 \times \cos\alpha$. From this rule, it can be seen that the larger the forming angle, the smaller the thickness t of the deformation zone, the higher the thinning rate, and the easier it is to break. When α reaches a certain value, the deformation zone was cracked. At this time, the angle α can be used as a judgment value of whether the sheet metal was broken. The larger the forming limit angle, the greater the amount of deformation that the sheet can produce, and the higher the forming performance. In the experiment, the forming limit angle was used as the standard for the forming performance of the material[25-27].

After orthogonal experiment, the forming limit angle α_{max}(°) and temperature T(°C) were obtained (Table 5).

Table 5 Orthogonal test data table

Run	A	B	A×B	C	A×C	B×C	α_{max}	T
1	500	1	3	12	3	1	29	52
2	500	2	1	8	1	2	23	61
3	500	1.5	2	16	2	3	27	60
4	1000	1	1	12	1	1	36	87
5	1000	2	2	8	2	2	41	90
6	1000	1.5	3	16	3	3	13	110
7	1500	1.5	2	12	1	1	59	80
8	1500	1	3	8	2	2	47	100
9	1500	2	1	16	3	3	56	112
10	2000	2	2	16	3	1	71	140
11	2000	1.5	3	12	1	2	62	110
12	2000	1	1	8	2	3	49	95
13	2500	2	3	12	2	1	59	120
14	2500	1.5	1	8	3	2	51	100
15	2500	1	2	16	1	3	55	120
16	3000	1.5	1	8	2	1	64	130
17	3000	1	2	16	3	2	65	125
18	3000	2	3	12	1	3	52	135

Table 5 was imported into SPSS software for orthogonal test variance analysis. The results are shown in Table 6.

Table 6 Orthogonal test results data analysis

Factor	Mean difference	Degrees of freedom	F	Sig	Distinctiveness
A	560.633	5	21.425	0.045	Important
B	33.500	2	1.280	0.439	Not important
C	32.000	2	1.223	0.450	Not important
A×B	4.081	2	0.156	0.865	Not important
B×C	80.082	2	3.061	0.246	Not important
A×C	0.333	2	0.013	0.987	Not important

According to the data analysis table of the orthogonal test results, the effects of the three main factors and their interaction on the forming limit angle are A>B×C>B>C>A×B>A×C. the rotational speed has the most significant effect on the forming angle, and other factors have less effect. It can be seen from Fig. 9 that the forming limit angle is gradually increased sharply from 500prm to 2000prm with the spindle speed is increased, but after 2000prm, the forming limit angle is basically unchanged, the forming ability of magnesium alloy has been greatly improved compared with 500prm. Generally speaking, the forming ability is increased with the rotational speed is increased. After rotational speed is reached a certain speed, the forming ability is basically unchanged. The forming limit angle gradually is decreased with the vertical step size is increased, but the change range is small. The forming limit angle is also increased only slightly with the tool diameter is increased, with a change of about 5°, the forming ability is basically unchanged. According to the optimal parameters, rotational speed is 2000prm, vertical step size is 1mm, and the tool diameter is 16mm, the forming limit angle can be up to 76°.

It can be seen from the influence of each process parameter on the temperature at the forming limit angle that the rotational speed, vertical step size, and the tool diameter is increased will increase its temperature. The most important factor is the rotational speed. As the speed is increased, the temperature is doubled, and the trend of temperature increase is roughly the same as the trend of forming ability. The vertical step size and tool diameter have little effect on the temperature, and the change is about 10°C.

The influence of various process parameters on the forming ability and temperature is analyzed, and the conclusion is that the forming ability and temperature change trend is basically the same as the temperature is increased, but the vertical step size is different, as the vertical step size is increased, the forming capacity gradually decreases, but the temperature is increased. The main reason is that the vertical step size is increased within this range, the pressure of the sheet is increased, causing the sheet is broken, and the forming ability is reduced. At this time, the influence of pressure on the plate is greater than the influence of temperature increase on the sheet forming capacity.

The rotational speed is the biggest factor affecting the forming limit angle. When the speed is increased above 2000prm, the forming ability is not changed basically. When the speed is increased, the temperature will increase, reducing the service time of the forming tool. In the experiment, it was also

found that when the temperature is increased, the outer surface of the parts will have "ripple marks", which makes the surface quality poor, as shown in Fig. 10. 2000prm is the best choice for other deformation characteristics experiments.

Vertical step size is an important factor that affects forming efficiency. As the vertical step size is increased, the processing time is reduced and the production efficiency is improved, but at the same time the surface roughness will be increased. The vertical step size is small, which is helpful to reduce the surface roughness of the parts, but the processing time will be increased.

The tool diameter has little effect on the forming ability. The tool diameter is increased will increase the contact area between the forming tool and the sheet, the temperature will be increased, and the forming ability will be increased. The lower tool diameter will cause more serious damage to the plate, thus forming capacity is reduced. On the other hand, the tool diameter is too large and the corners of the formed parts are not easy to form, therefore, the choice of forming tool diameter depends on the complexity of the forming part.

3.2 Deformation and geometrical accuracy in FHIF

In order to better understand the deformation characteristics and geometrical accuracy of the early, intermediate and final forming stages, the ideal model and the contour drawing of the actual part cross section were extracted from CATIA for comparison, as shown in Fig. 11. Due to the symmetry of the part, only the half-part contour is analyzed. When the part is above the CAD model, it is "+", otherwise it is "□".

It can be seen from the comparison of the cross-sectional views of the CAD model and the part that the edge area of the part will be bended to varying degrees in each period, which is caused by the blank holder. This mainly depends on the distance between the clamping edge and the contact position of the forming tool. The bend is particularly obvious in the early stage, and the 45° sidewall area is not obvious, there are no obvious upper and lower corners, this is the shortcoming of no lower mold. Through analysis, it is found that there are defect in the lower corners in each period, which is left during the last round of the forming tool. The forming tool squeezes the metal and flows to the side edge, so that the metal is not deformed piled up, so the thickness of this part will be thicker. And the bottom of the part is not flat, and the center position is higher than the edge position, this is because during the local plastic deformation process, the bottom edge position is subjected to more downward pressure on the tool head, so that the center of the bottom is always higher than the position where the forming tool is being processed during the entire process.

3.3 Thickness distribution in FHIF

Comparing the simulated thickness results with the actual results, it can be seen from Fig. 12 that the thickness of the sidewall area is not uniform in the early stage of forming, and the uniform thickness is 0.99mm in the intermediate and final stages of forming, which is 11% thinner than the theoretical

thickness of 1.13mm. Friction heating requires rotating contact friction between the tool head and the plate, material loss occurs, and it is impossible to use 100%, from the overall error analysis above, it can be seen that the thickness of the side wall region is partially thinned because part of the side wall material is squeezed into the bottom region. The experiment found that the thinning rate is basically the fixed value is 11%, so 89% of the theoretical sidewall thickness is the thickness of the actual FHIF sidewall uniform area.

It is found that the designed simulation model can accurately predict the thinning trend, but because the metal flow in the entire process cannot be accurately simulated, the trend can only be predicted, and the thickness and the true value are somewhat different. In the simulated parts, the thickness of the corners found during the experimental research was rapidly reduced. Due to the symmetry of the parts, the thickness profile (Fig. 13) only studies half-sections. In the unformed area, the sheet thickness is about 1.6 mm, and the sheet thickness was decreased rapidly in the upper fillet area, in the side wall area, as the forming depth was increased, the thickness of the plate gradually was stabilized. The stable thickness is about 1.13mm, which is not much different from the theoretical thickness, which is in accordance with the cosine law of the plate.

The measured thickness distribution along the forming depth in the final forming is as shown in Fig.14, it can be seen that the side wall area of the part does not reach a stable thickness at the beginning, but the thickness reaches a minimum after a certain forming depth. Through experiments, it is found that the forming thickness reaches a stable thickness when the forming depth is about 15mm, and the temperature also reaches a stable value, so in the forming process, special attention should be paid to forming depth 0-15mm, which is the easiest to break.

3.4 Strain and stress distribution in FHIF

Due to the nature and complexity of the process, it is impossible to obtain the stress state in the FHIF process. Therefore, the equivalent stress was evaluated by the finite element method. The stress evolution at each forming stage of the forming process is shown in Fig. 15. It can be observed that the maximum stress value was increased as the forming stage was increased. For the early forming stage, the value is 165.1MPa, 171.1MPa in the intermediate stage, and 174.2MPa in the final forming stage. The maximum strain of the part in the early forming stage is 0.437, while the plastic strain of the part in the intermediate forming stage and the final forming stage has increased but has not changed much, both are around 0.471. The strain measured in the side wall area is basically fixed by grid experiment.

The plastic strain value increases from the early stage to the middle stage of forming, but the plastic deformation does not change much from the middle stage to the final stage of forming, because the sidewall region at this stage is the maximum equivalent strain value, and the thickness of the sidewall region basically does not occur variety. The amount of strain changes from the beginning to the early stage is large, and then basically unchanged. Corresponding to the existence of a depth in the above experiment, after this depth the sheet will be basically not break.

4 Conclusions

(1) For the FHIF of frictional heat, the forming limit angle can be up to 76°. The most obvious way to increase the forming limit angle is to increase the rotational speed, but after increasing to 2000prm, the forming capacity does not increase much and serious defects will occur. The amount is an important factor that affects the forming efficiency. The tool diameter determines the size of the corner of the formed part.

(2) In the FHIF process, due to the limitations of the experimental conditions, it will be different from the ideal model. The bending phenomenon first occurs in the early stage of forming, which makes the upper corner part have the worst accuracy, and the lower corner part has obvious convex marks.

(3) The side wall stabilization area of the actual part is 11% thinner than the theoretical stable thickness. The side wall area of the part does not reach the stable thickness at the beginning, but the thickness is minimized at the forming depth of about 15mm, so the forming process should pay special attention to when the forming depth is 0-15mm, which is the most prone to cracking.

Declarations

Acknowledgments

The authors sincerely thanks to Professor Liuru Zhou of Nanchang University for his critical discussion and reading during manuscript preparation.

Funding

Supported by National Natural Science Foundation of China (Grant No. 51465038)

Biographical notes

Jiahao Wang, born in 1996, is currently a postgraduate at *Nanchang University, China*.

E-mail: 15839628631@163.com

Liuru Zhou, born in 1963, is currently a PhD associate professor *at Nanchang University, China*. His research interests include sheet metal incremental forming theory and simulation.

E-mail: zlrhust@163.com

Shiyao Hu, born in 1995, is currently a postgraduate at *Nanchang University, China*.

E-mail: 1069154665@qq.com

References

1. J Lee, H J Bong, Y S Lee, et al. Pulsed electric current V-bending springback of AZ31B magnesium alloy sheets. *Metallurgical and Materials Transactions*, 2019, 50(A):2720-2731.
2. N Duc-Toan, Y Seung-Han, J Dong-Won, et al. A study on material modeling to predict spring-back in V-bending of AZ31 magnesium alloy sheet at various temperatures. *International Journal of Advanced Manufacturing Technology*, 2012, 62:551-562.
3. J Yanagimoto, K Oyamada, T Nakagawa, Springback of high-strength steel after hot and warm sheet formings, *CIRP Annals - Manufacturing Technology*. 2005, 54(1): 213–216.
4. R Neugebauer, T Altan, M Geiger, M Kleiner, A Sterzing, Sheet metal forming at elevated temperatures, *CIRP Annals - Manufacturing Technology*. 2006, 55(2): 793–816.
5. J Jeswiet, F Micari, G Hirt, et al. Asymmetric Single Point Incremental Forming of Sheet Metal. *CIRP Annals - Manufacturing Technology*, 2005, 54(2):88-114.
6. W C Emmens, A H van den Boogaard. An overview of stabilizing deformation mechanisms in incremental sheet forming. *Mater Process Technol*, 2009, 209(8):3688–3695.
7. P Shrivastava, P Tandon. Microstructure and texture based analysis of forming behavior and deformation mechanism of AA1050 sheet during Single Point Incremental Forming. *Journal of Materials Processing Technology*, 2019, 266:292-310.
8. T J Kim, D Y Yang. Improvement of formability for the incremental sheet metal forming process. *InternationalJournal of Mechanical Sciences*, 2000, 42(7): 1271-1286.
9. M B Silva, P S Nielsen, Bay N, et al. Failure mechanisms in single-point incremental forming of metals. *The International Journal of Advanced Manufacturing Technology*, 2011, 56(9-12):893-903.
10. K A Al-Ghamdi, G Hussain. Threshold tool-radius condition maximizing the formability in SPIF considering a variety of materials: Experimental and FE investigations. *International Journal of Machine Tools & Manufacture*, 2015, 88:82-94.
11. J Jeswiet, F Micari, G Hirt, et al. Asymmetric Single Point Incremental Forming of Sheet Metal. *CIRP Annals - Manufacturing Technology*, 2005, 54(2):88-114.
12. Güler, Baran, M Efe. Forming and Fracture Limits of Sheet Metals Deforming without a Local Neck. *Journal of Materials Processing Technology*, 2017, 252, 477–484.
13. S Ai, B Lu, J Chen, et al. Evaluation of deformation stability and fracture mechanism in incremental sheet forming. *International Journal of Mechanical Sciences*, 2017, 124–125:174-184.
14. B H Ramzi, T Sebastien, R Fabrice, et al. Numerical Prediction of the Forming Limit Diagrams of Thin Sheet Metal using SPIF Tests. *Procedia Engineering*, 2017, 183:113-118.
15. Y Li, X Chen, Z Liu, et al. A review on the recent development of incremental sheet-forming process. *The International Journal of Advanced Manufacturing Technology*, 2017, 92:2439-2462.
16. T Husmann, C S Magnus. Thermography in incremental forming processes at elevated temperatures. *Measurement*, 2016, 77:16-28.
17. André Leonhardt, G Kurz, José Victoria-Hernández, et al. Experimental study on incremental sheet forming of magnesium alloy AZ31 with hot air heating. *Procedia Manufacturing*, 2018, 15:1192-

1199.

18. W Bao, X Chu, S Lin, et al. Experimental investigation on formability and microstructure of AZ31B alloy in electropulse-assisted incremental forming. *Materials & Design*, 2015.
19. Q Zhang, F Xiao, H Guo, et al. Warm negative incremental forming of magnesium alloy AZ31 Sheet: New lubricating method. *Journal of Materials Processing Tech*, 2010, 210(2):323-329.
20. M Zhenghua. Formability of AZ31 Magnesium Alloy Sheet under Warm and Electromagnetic Forming Condition. *China Mechanical Engineering*, 2011, 22(2):239-242.
21. S Zhang, G H Tang, W Wang, et al. Evaluation and optimization on the formability of an AZ31B Mg alloy during warm incremental sheet forming assisted with oil bath heating. *Measurement*, 2020, 157:107673.
22. D Xu, B Lu, T Cao, A comparative study on process potentials for frictional stir- and electric hot-assisted incremental sheet forming, *Procedia Engineering*, 2014, 81:2324-
23. M S Shim, J J Park. The formability of aluminum sheet in incremental forming. *Journal of Materials Processing Technology*, 2001, 113(1-3):654-658.
24. J J Park, Y H Kim. Fundamental studies on the incremental sheet metal forming technique. *Journal of Materials Processing Technology*, 2003, 140(1-3):447-453.
25. M Otsu, Excellent formability of light metals sheets by friction stir incremental forming, *Key Eng. Mater*. 2016, 716: 3–10.
26. J R Duflou, J Verbert, B Belkassem, et al, Process window enhancement for single point incremental forming through multi-step toolpaths, *CIRP Annals - Manufacturing Technology*. 2008, 57:253–256.
27. A Mulay, S Ben, S Ismail, A Kocanda, Experimental investigations into the effects of SPIF forming conditions on surface roughness and formability by design of experiments, *Dissertations & Theses – Gradworks*, 2017, 39:1–14.

Figures

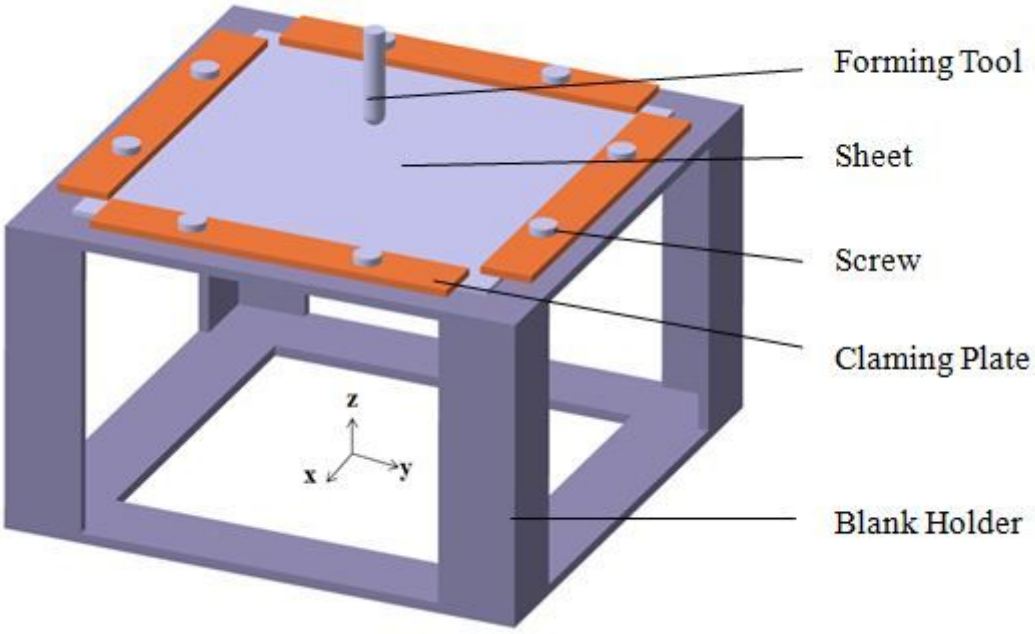

Figure 1

FHIF setup

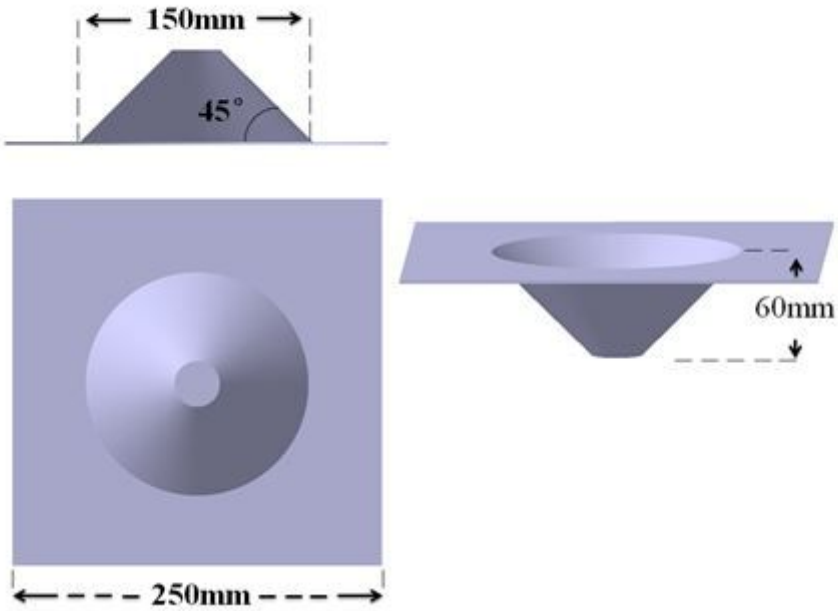

Figure 2

CAD model

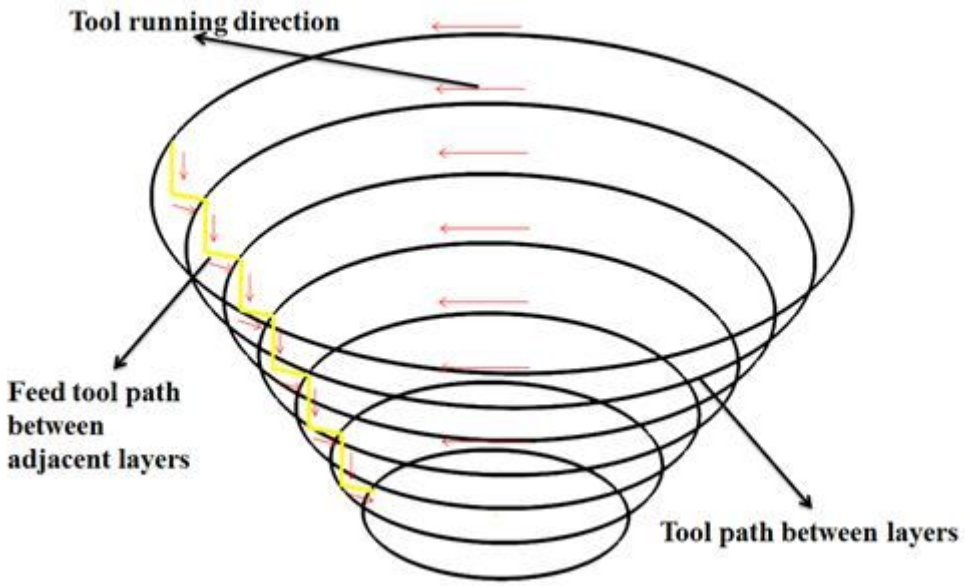

Figure 3

Tool path

HIF Stage	CAD model	Formed FHIF parts
Early		
Intermediate		
Final	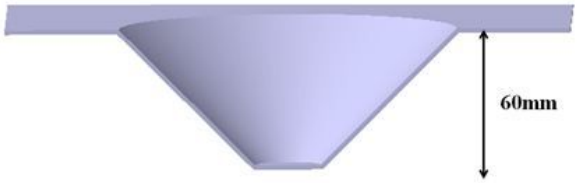	

Figure 4

Geometric models and formed parts

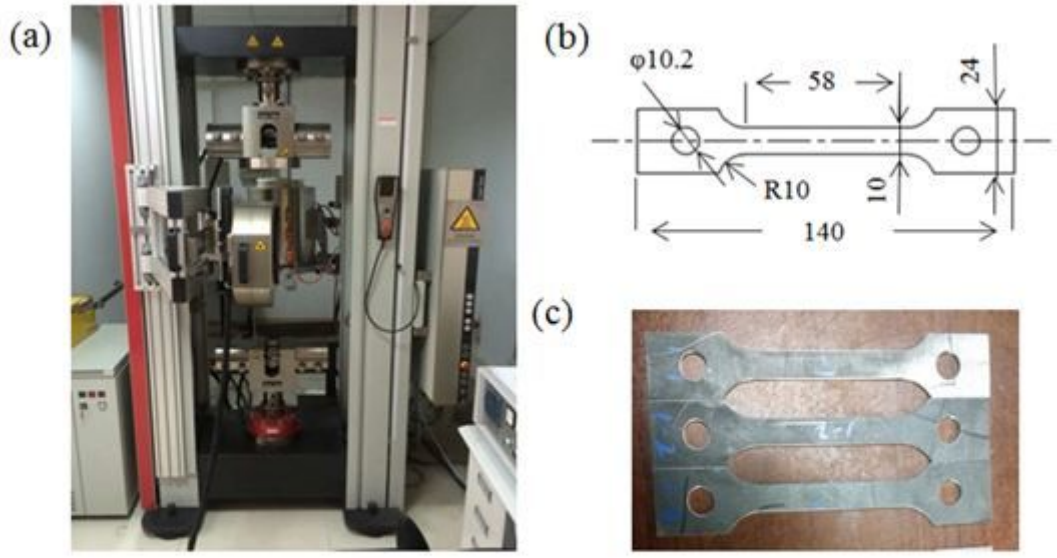

(a) Universal material testing machine

(b) Dimension details of dog bone samples

(c) Test samples

Figure 5

Mechanical characterization of AZ31B sheet material

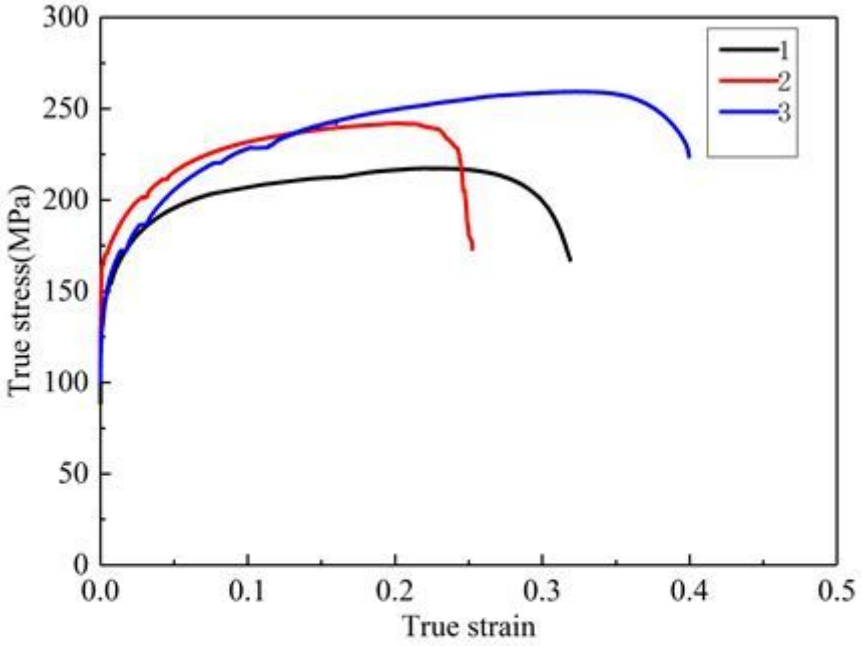

Figure 6

True stress-strain curves

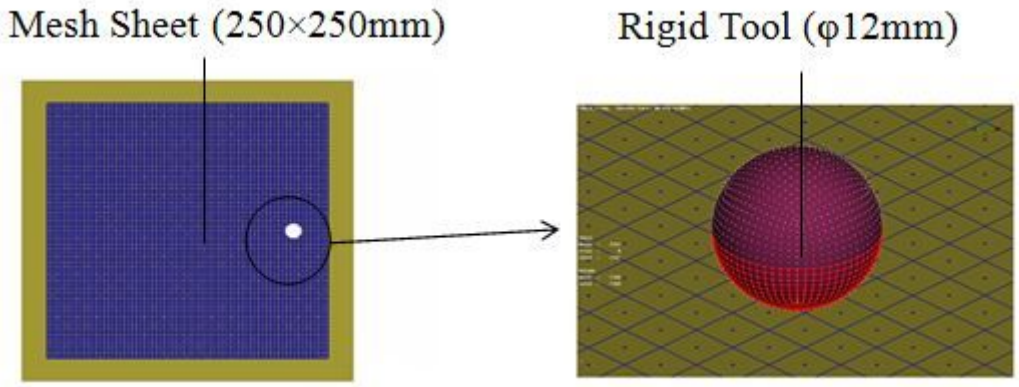

Figure 7

Meshed sheet and forming tool

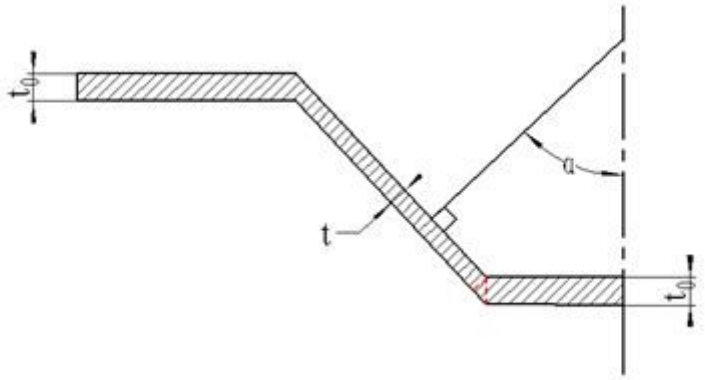

Figure 8

Schematic diagram of thickness and forming angle

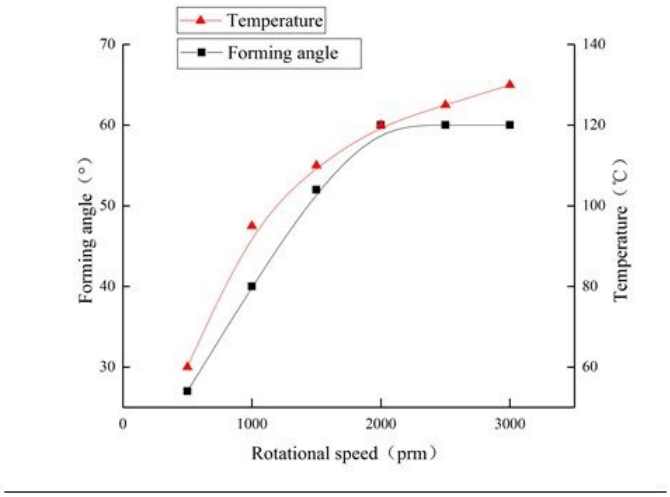

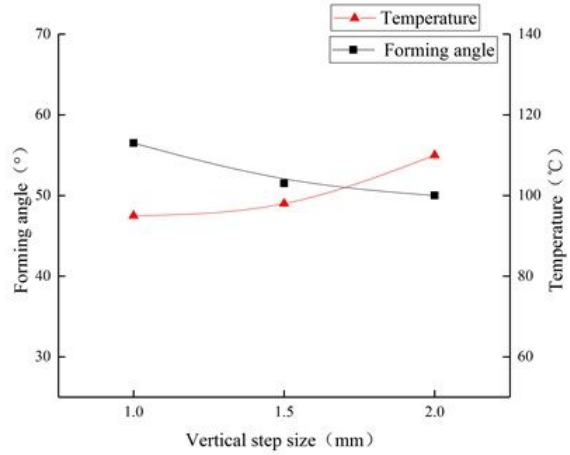

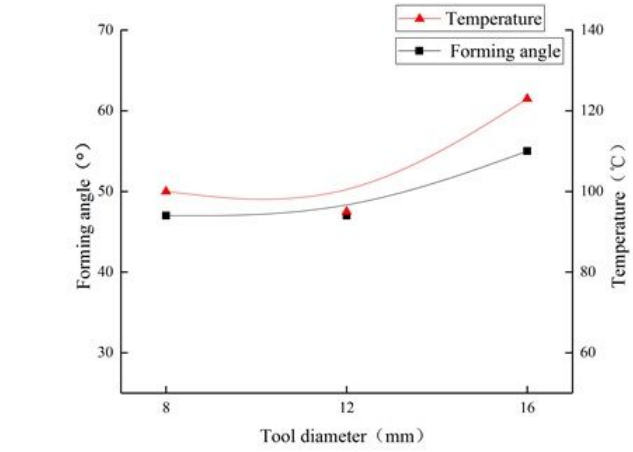

Figure 9

Influence of forming parameters

Figure 10

Forming defects

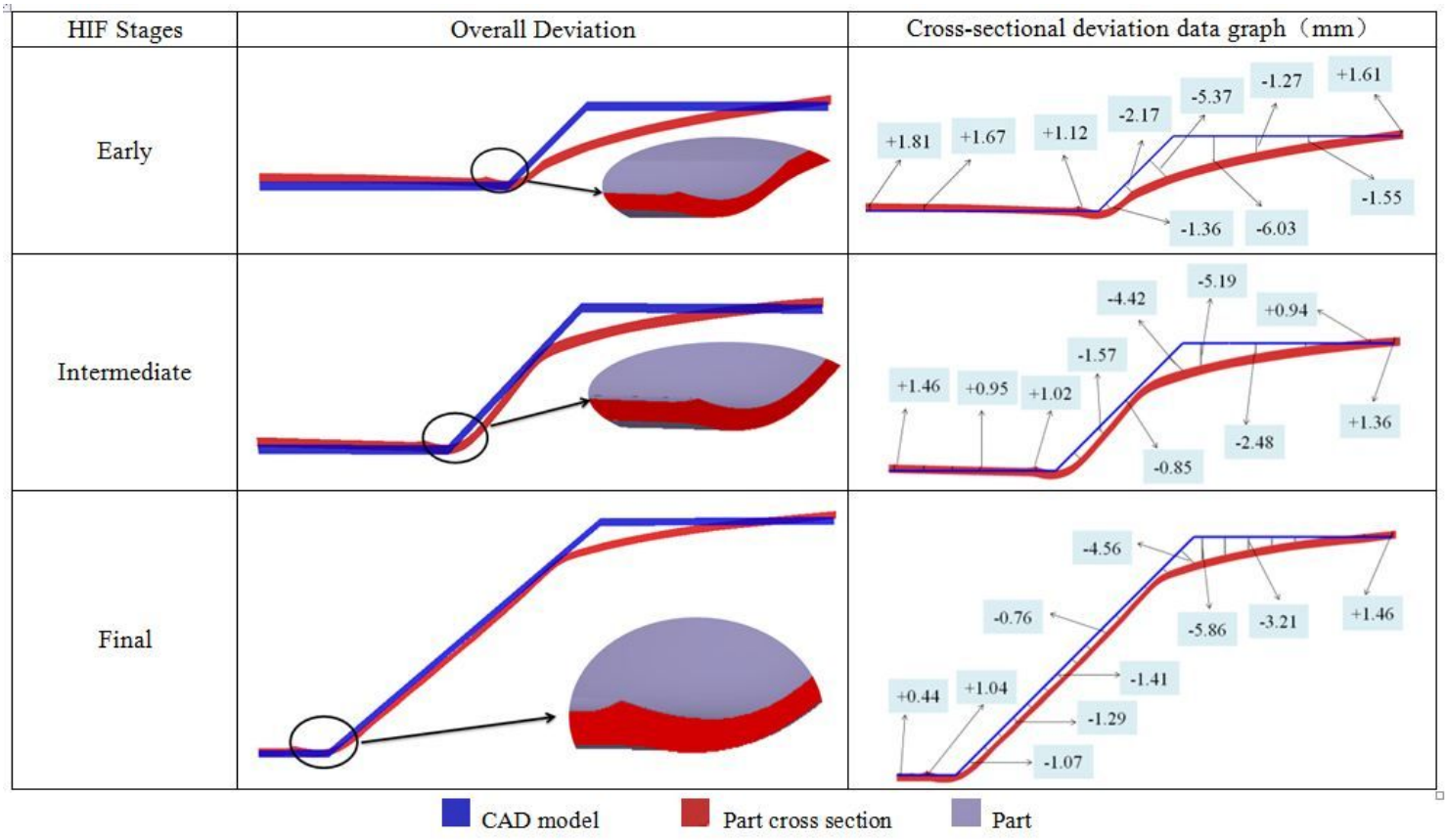

Figure 11

Outline drawing of cross section

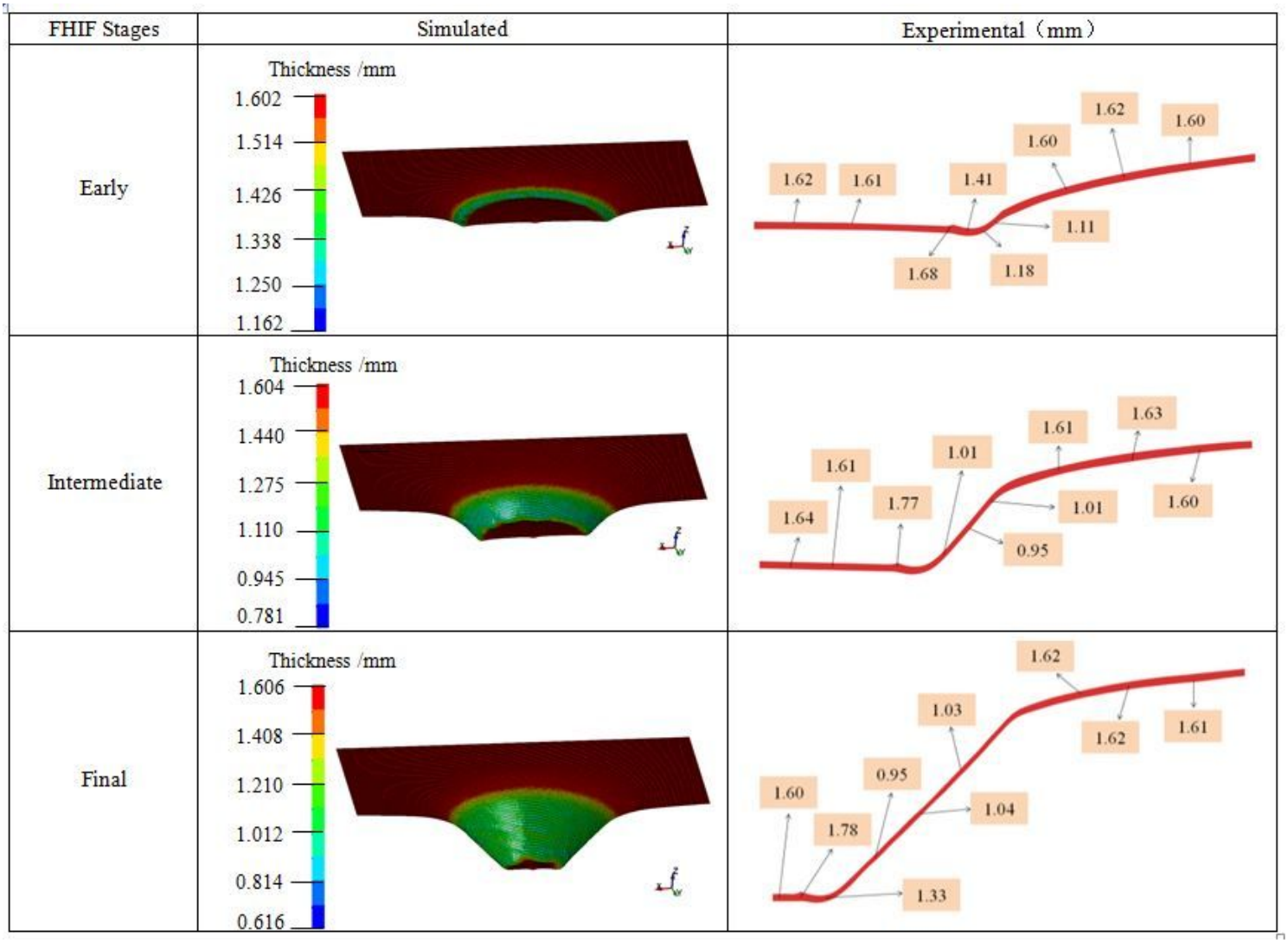

Figure 12

Simulated and experimental wall thickness distribution in FHIF parts resulted in different deformation stages

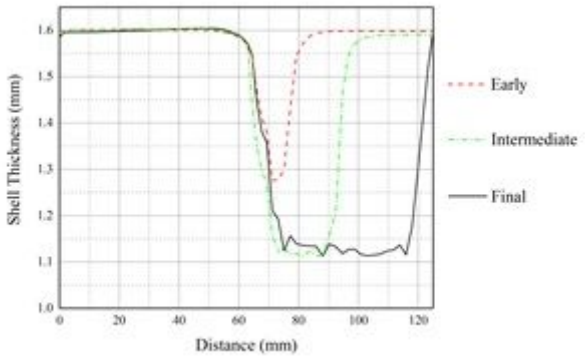

Figure 13

Cross-sectional thickness distribution

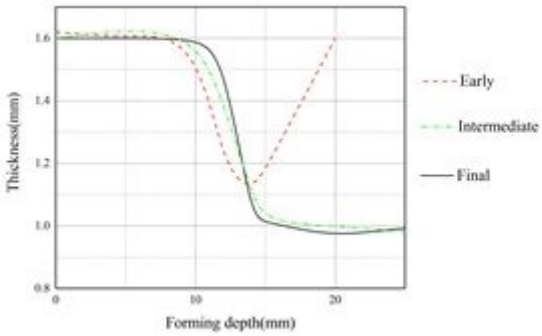

Figure 14

Thickness with the forming depth

FHIF Stages	Simulated Equivalent Stress	Simulated Plastic Strain
Early	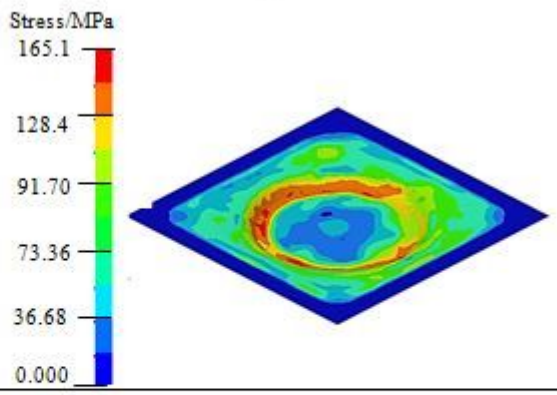	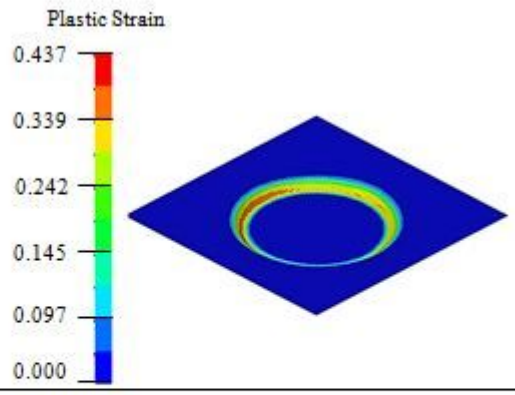
Intermediate	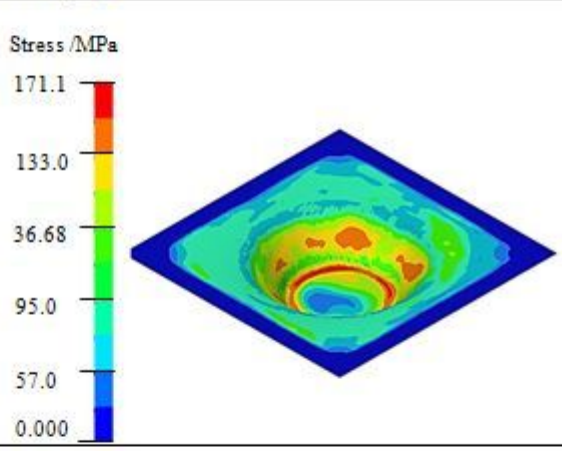	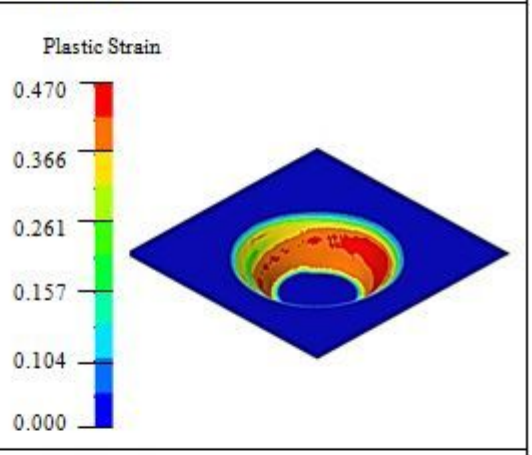
Final	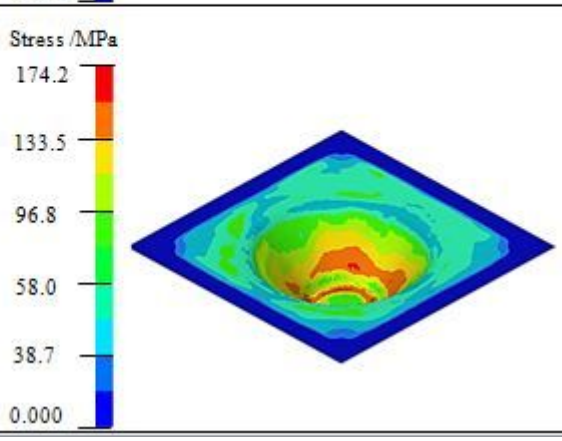	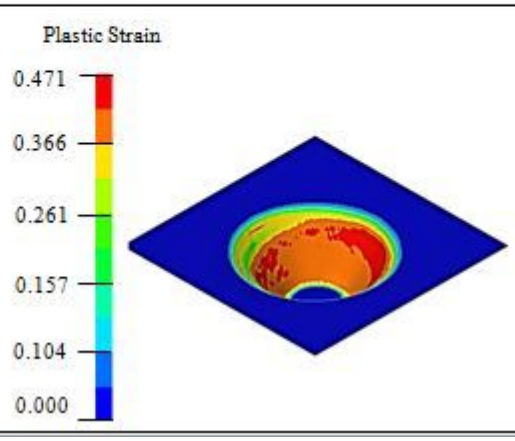

Figure 15

Simulated stress and plastic strain distribution in FHIF